CMI

www.nature.com/cmi

ARTICLE

MST4 kinase regulates immune thrombocytopenia by phosphorylating STAT1-mediated M1 polarization of macrophages

Jingjing Cao[1,9], Lili Ji[1,9], Yanxia Zhan[1,9], Xia Shao[1,2], Pengcheng Xu[1,2], Boting Wu[3], Pu Chen[4], Luya Cheng[1], Xibing Zhuang[1,2], Yang Ou[1,2], Fanli Hua[5], Lihua Sun[5], Feng Li[1,5], Hao Chen[6]✉, Zhaocai Zhou[7]✉ and Yunfeng Cheng[1,2,5,8]✉

Primary immune thrombocytopenia (ITP) is an autoimmune hemorrhagic disorder in which macrophages play a critical role. Mammalian sterile-20-like kinase 4 (MST4), a member of the germinal-center kinase STE20 family, has been demonstrated to be a regulator of inflammation. Whether MST4 participates in the macrophage-dependent inflammation of ITP remains elusive. The expression and function of MST4 in macrophages of ITP patients and THP-1 cells, and of a macrophage-specific *Mst4*$^{-/-}$ (*Mst4*$^{\Delta M/\Delta M}$) ITP mouse model were determined. Macrophage phagocytic assays, RNA sequencing (RNA-seq) analysis, immunofluorescence analysis, coimmunoprecipitation (co-IP), mass spectrometry (MS), bioinformatics analysis, and phosphoproteomics analysis were performed to reveal the underlying mechanisms. The expression levels of the *MST4* gene were elevated in the expanded M1-like macrophages of ITP patients, and this elevated expression of *MST4* was restored to basal levels in patients with remission after high-dose dexamethasone treatment. The expression of the *MST4* gene was significantly elevated in THP-1-derived M1 macrophages. Silencing of *MST4* decreased the expression of M1 macrophage markers and cytokines, and impaired phagocytosis, which could be increased by overexpression of *MST4*. In a passive ITP mouse model, macrophage-specific depletion of *Mst4* reduced the numbers of M1 macrophages in the spleen and peritoneal lavage fluid, attenuated the expression of M1 cytokines, and promoted the predominance of FcγRIIb in splenic macrophages, which resulted in amelioration of thrombocytopenia. Downregulation of *MST4* directly inhibited STAT1 phosphorylation, which is essential for M1 polarization of macrophages. Our study elucidates a critical role for MST4 kinase in the pathology of ITP and identifies MST4 kinase as a potential therapeutic target for refractory ITP.

Keywords: Primary immune thrombocytopenia; Mammalian sterile-20-like kinase 4 (MST4); Macrophages; M1 polarization; Signal transducer and activator of transcription-1 (STAT1)

Cellular & Molecular Immunology (2023) 20:1413–1427; https://doi.org/10.1038/s41423-023-01089-8

INTRODUCTION

Primary immune thrombocytopenia (ITP) is an acquired autoimmune bleeding disorder in which autoantibody-opsonized platelets are prematurely cleared in the spleen and/or liver by macrophages [1–4]. Abnormal immune responses and defective immune tolerance, which can include a skewed Th1/Th2 balance, defective regulatory T cells (Tregs), and abnormal activation of cytotoxic T cells, are considered to play crucial roles in the pathogenesis of ITP [1, 5–10].

Macrophages, which play multiple roles in both innate and adaptive immune responses, can polarize into classically activated M1 macrophages or alternatively activated M2 macrophages depending on the environmental stimuli [11–15]. After induction by key transcription factors, such as interferon regulatory factor 5 (IRF5), signal transducer and activator of transcription-1 (STAT1), and IRF3, M1 macrophages express a high level of proinflammatory cytokines, phagocytose pathogens, and induce potent pathogenic Th1 and Th17 responses [16, 17]. Immunosuppressive M2 macrophages produce anti-inflammatory cytokines and direct the Th2 response. Substantial expansion of M1 macrophages has been observed in the spleen of ITP patients and in the peripheral blood of pediatric ITP patients [18, 19], but its specific roles in ITP have not been fully elucidated. Macrophages phagocytose IgG-opsonized platelets via Fcγ receptors (FcγRs), which consist of activating and inhibitory FcγRs [5, 20]. Fine-tuning of the activating and inhibitory FcγR balance is critical in clearing the pathogen-IgG

[1]Department of Hematology, Zhongshan Hospital, Fudan University, Shanghai 200032, China. [2]Center for Tumor Diagnosis & Therapy, Jinshan Hospital, Fudan University, Shanghai 201508, China. [3]Department of Transfusion Medicine, Zhongshan Hospital, Fudan University, Shanghai 200032, China. [4]Department of Laboratory Medicine, Zhongshan Hospital, Fudan University, Shanghai 200032, China. [5]Department of Hematology, Zhongshan Hospital Qingpu Branch, Fudan University, Shanghai 201700, China. [6]Department of Thoracic Surgery, Zhongshan-Xuhui Hospital, Fudan University, Shanghai 200031, China. [7]State Key Laboratory of Genetic Engineering, Zhongshan Hospital, School of Life Sciences, Fudan University, Shanghai 200438, China. [8]Institute of Clinical Science, Zhongshan Hospital, Fudan University, Shanghai 200032, China. [9]These authors contributed equally: Jingjing Cao, Lili Ji, Yanxia Zhan. ✉email: h.chen@fudan.edu.cn; zhouzhaocai@fudan.edu.cn; yfcheng@fudan.edu.cn

Received: 5 April 2023 Accepted: 23 September 2023
Published online: 13 October 2023

Table 1. Clinical characteristics of ITP patients

Patient no.	Sex	Age (years)	Platelet count ($\times 10^9$/L)		Treatment efficacy
			Pretreatment	Post-treatment	
ITP1	F	26	5	101	CR
ITP2	F	53	6	475	CR
ITP3	F	65	4	304	CR
ITP4	F	57	15	300	CR
ITP5	M	60	27	298	CR
ITP6	F	36	27	230	CR
ITP7	M	67	15	225	CR
ITP8	F	46	5	224	CR
ITP9	M	63	14	218	CR
ITP10	M	88	12	210	CR
ITP11	M	64	2	181	CR
ITP12	F	47	24	178	CR
ITP13	F	41	7	164	CR
ITP14	M	29	28	164	CR
ITP15	M	19	26	157	CR
ITP16	M	59	9	141	CR
ITP17	F	35	24	138	CR
ITP18	F	19	28	137	CR
ITP19	M	74	14	117	CR
ITP20	F	68	1	104	CR
ITP21	F	47	15	76	PR
ITP22	F	51	16	50	PR
ITP23	F	51	13	25	NR
ITP24	F	35	17	24	NR
ITP25	F	52	17	23	NR
ITP26	F	72	20	22	NR
ITP27	M	29	20	18	NR
ITP28	M	42	27	17	NR
ITP29	F	65	19	15	NR
ITP30	F	52	17	14	NR
	M:F = 11:19	51(35,64)	15(8,24)	139(24,219)	

ITP primary immune thrombocytopenia, *CR* complete response, *PR* partial response, *NR* no response

complex and dampening the exacerbated proinflammatory cytokine storm secondary to immune complex-associated inflammation [21–23]. An imbalance between activating and inhibitory FcγRs has been observed in patients with ITP [24, 25].

Mammalian sterile-20-like kinase 4 (MST4) [26, 27], also known as serine/threonine kinase 26, belongs to germinal center kinase (GCK) III of STE20-like kinases [28, 29]. MST4 plays diverse roles in various physiological conditions and diseases. We previously reported that MST4 regulates macrophage-dependent inflammation by modulating TRAF6 activity in the TLR4 signaling pathway [30]. Furthermore, MST4 could modulate the activity of the IκBα, ERK, JNK, and dectin-1/p-Syk signaling pathways in inflammatory responses [31, 32]. However, the potential role of MST4 in macrophage-related ITP pathology remains to be investigated.

The present study aimed to determine the pathological features of circulating M1 macrophages in ITP patients, to investigate the modulating roles of MST4 in the development and function of these macrophages and to explore the underlying molecular mechanisms that would shed light on the pathogenesis of ITP and novel strategies for treatment.

METHODS

Patients

Thirty primary ITP patients (11 males and 19 females; median age, 51 years; median platelet count, 15×10^9/L) were enrolled from January 2016 to December 2018 (Table 1). All patients met the diagnostic criteria proposed by an international working group [33] and received high-dose dexamethasone (HD-DXM; 40 mg/day for 4 consecutive days) if they had platelet counts lower than 30×10^9/L or significant bleeding. Blood samples were collected prior to HD-DXM therapy and on day 10 to evaluate the treatment response, which was classified as complete response (CR), partial response (PR), or no response (NR) based on the platelet count and bleeding events as previously described [34].

The healthy control (HC) cohort consisted of 20 healthy volunteers with a median age of 43 years and a median platelet count of 252×10^9/L. The phenotype of circulating M1-like macrophages was defined as $CD14^+CD86^+$ in the study according to a previous study [35]. CD14 MicroBeads (Miltenyi Biotec, Germany) were used to enrich M1-like macrophages with a purity >80% (Supplementary Fig. 1).

The study was approved by the Institutional Review Board of Zhongshan Hospital, Fudan University. Written informed consent was collected upon enrollment. The study was conducted in accordance with the Declaration of Helsinki.

Cell culture and polarization

Human monocytic THP-1 cells were maintained in RPMI-1640 medium supplemented with 10% heat-inactivated fetal bovine serum (FBS) and 50 pM ß-mercaptoethanol. THP-1 monocytes were induced to differentiate into M1 macrophages by incubation with phorbol 12-myristate 13-acetate (PMA; 100 ng/ml; Sigma–Aldrich, Darmstadt, Germany) for 48 h, resting in complete medium for 24 h, and incubation with LPS (100 ng/ml; Sigma–Aldrich) + IFN-γ (20 ng/ml; PeproTech, Rocky Hill, NJ, USA) for 24 h.

The magnetically sorted $CD14^+$ monocytes were maintained in RPMI-1640 medium supplemented with 10% FBS and granulocyte-macrophage colony-stimulating factor (GM-CSF; 20 ng/ml; PeproTech, Rocky Hill, NJ, USA) for 5 d to drive monocyte differentiation toward an M1 phenotype and then stimulated with LPS (100 ng/ml; Sigma–Aldrich) + IFN-γ (20 ng/ml; PeproTech, Rocky Hill, NJ, USA) for 24 h.

Lentivirus transfection of THP-1 cells

For the knockdown of *MST4*, *MST4*-specific short hairpin RNA (shRNA, target sequence: CCAGATTGCTACCATGCTAAA) and control shRNA (with scrambled sequence) were constructed with a GPH vector. For the overexpression of *MST4*, cDNA of human *MST4* (ID: 51765 NM_006281.2) was cloned and inserted into the lentiviral vector GTP-C-3flag, and an empty vector (EV) was used as the control. THP-1 cells were transduced with lentivirus (multiplicity of infection = 50) and selected in the presence of puromycin (2.5 μg/ml; Sigma–Aldrich). The transfection efficiency was validated by RT–qPCR and Western blotting analyses (Supplementary Fig. 2).

Animals

C57BL6 mice with two loxP sites flanking exon 8 of the *Mst4* gene ($Mst4^{fl/fl}$) were crossed with lysozyme M (Lyz2) Cre-recombinase "knock-in" mice to generate mice with myeloid deficiency of *Mst4* ($Mst4^{fl/fl}$ $Lyz2^{cre/wt}$, termed $Mst4^{\Delta M/\Delta M}$ mice) (Supplemental Fig. 3A). The efficiency of *Mst4* deletion in macrophages was confirmed by qRT–PCR and immunoblot analyses of splenic macrophages and bone marrow-derived macrophages (BMDMs) (Supplementary Fig. 3B, C). The animal care and procedures were approved by the Animal Care and Use Committee of Zhongshan Hospital, Fudan University.

Passive ITP model

The murine passive ITP model was established according to a previously described protocol [36]. Briefly, age- and sex-matched female mice (aged 6–8 weeks; platelet count range, $1000–1500 \times 10^9$/L) were injected with an anti-platelet monoclonal antibody (mAb; rat anti-mouse CD41, clone MWReg30; BD Biosciences, San Jose, CA, USA) at a dose of 68 μg/kg body weight for the first 2 days. For the subsequent 4 days, the dose was increased by 34 μg/kg each day. The mice were sacrificed on day 6 (24 h after the last injection of mAb).

The course of ITP development was evaluated by detecting the platelet count before injection and sacrifice. Briefly, whole-blood samples (5 μl) were collected from the saphenous vein, mixed with 45 μl of 2 mg/ml heparin, and counted using a Mindray BC-5300 Auto Hematology Analyzer.

Sample collection and processing

The spleen, bone marrow, and cells from peritoneal lavage fluid were collected at the time of sacrifice. $F4/80^+$ cells were magnetically isolated from splenocytes. M1 macrophages were generated by culturing bone marrow cells with RPMI-1640 medium supplemented with 10% FBS and 30% L929 cell supernatant for 7 days and then stimulated with 100 ng/ml LPS and 20 ng/ml IFN-γ for 24 h.

Flow cytometry analysis

For flow cytometric analysis, single-cell suspensions were stained with the indicated antibodies according to the manufacturer's instructions. Flow cytometric analysis was conducted using a BD FACSAriaIII (BD Biosciences), and the obtained data were analyzed with FlowJo software (FlowJo LLC, Ashland, OR, USA).

PBMCs and M1 macrophages derived from transfected THP-1 monocytes were stained with surface APC-CD14 and percpcy5.5-CD86 according to the manufacturer's instructions. For analysis of the phenotype of cells harvested from the peritoneum, spleen, and BMDMs, Fc receptors were blocked using anti-mouse CD16/32, and the cells were stained with surface FITC-CD11b, surface PE-F4/80, surface PE-Dazzle 594-CD86 and intracellular PE-Cy7-CD206. Mouse Fcγ receptors were detected by staining the cells with surface APC-CD32, APC-Cy7-CD16, and BV421-CD64 plus surface PE-F4/80, surface PE-Dazzle 594-CD86 and intracellular PE-Cy7-CD206 without blocking Fc receptors. PE-F4/80 was purchased from BD Pharmingen (San Jose, CA, USA), and other antibodies were purchased from BioLegend (San Diego, CA, USA).

RNA extraction, reverse transcription, and qRT-PCR

Total RNA from cells was extracted using an RNAiso Plus kit (Takara, Tokyo, Japan) and reverse-transcribed using Strand cDNA Synthesis SuperMix (Yeason, Shanghai, China) according to the manufacturer's instructions. qRT–PCR analysis was conducted using SYBR Green Master Mix (Yeason) with a QuantStudio 5 Real-time PCR system (Applied Biosystems, Foster City, CA, USA). Relative gene expression levels were calculated using the comparative cycle threshold method ($2^{-DeltaDeltaCt}$) and normalized to the level of β-actin. The primer sequences are listed in Supplementary Table 1 and Supplemental Table 2.

RNA sequencing (RNA-seq) analysis

Sorted splenic macrophages ($>5 \times 10^6$) were collected from $Mst4^{\Delta M/\Delta M}$ and $Mst4^{fl/fl}$ ITP mice. Total RNA was extracted with TRIzol (Thermo Fisher, Rockford, IL, USA). The RNA amount, purity, and integrity of each sample were assessed, and high-quality RNA (RIN > 7.0) was used to construct the RNA-seq transcriptome libraries.

Differentially expressed genes (DEGs) between samples from $Mst4^{\Delta M/\Delta M}$ and $Mst4^{fl/fl}$ ITP mice were identified by calculating the expression levels of each transcript with the transcripts per million method. The R package DEseq2 was used for differential expression analysis. For MA plots, log2-fold changes and log2-normalized counts were calculated using DEseq2. Significant DEGs were defined based on an absolute value of the logarithmic fold change >1 and a false discovery rate <0.05. KEGG analysis was performed using the ClusterProfiler package. Gene set enrichment analysis (GSEA) was performed with the KEGG and hallmark gene sets from the Molecular Signatures Database (http://software.broadinstitute.org/gsea/msigdb/).

Macrophage phagocytic assay

A phagocytosis assay of BMDM-derived macrophages was performed using platelets obtained from wild-type C57/BL6 mice. Freshly isolated platelets ($100 \times g$, 10 min) were labeled with 10 μM 5-chloromethylfluorescein diacetate (Yeason) at 37 °C for 2 h and then incubated with 10 μg of rat anti-mouse CD41 monoclonal antibody (Thermo Fisher) at room temperature for 30 min. The rat anti-mouse CD41 mAb-coated platelets (termed antibody-coated platelets) were incubated with macrophages at a ratio of 1:100 at 37 °C for 2 h. In the confocal laser microscopy experiments, the cells were stained with Hoechst and analyzed by confocal laser microscopy. For flow cytometry, the cells were quenched for surface fluorescence with Trypan blue and then stained with surface APC-CD61 (BioLegend) to label platelets that had not been engulfed by macrophages. In the FACS analysis, the phagocytic index was defined as the ratio of antibody-opsonized platelet-positive macrophages at 37 °C to that at 4 °C.

A phagocytosis assay of THP-1-derived macrophages was performed using a Phagocytosis Assay kit (Cayman Chemical, Ann Arbor, MI, USA) according to the manufacturer's protocol. Briefly, IgG-coated latex beads were incubated with M1 macrophages at 1:400 dilution (for FACS analysis) or 1:100 dilution (for confocal laser microscopy analysis) for 2 h at 37 °C. Negative control samples, which were needed for FACS analysis, were incubated with IgG-coated latex beads at 4 °C for 2 h. In the confocal laser microscopy experiments, the cells were stained with Hoechst for 10 min at 37 °C following the manufacturer's instructions. Finally, the cells were washed twice and analyzed by flow cytometry or confocal laser microscopy. In FACS analysis, the phagocytic index was defined as the ratio of IgG-coated latex bead-positive macrophages at 37 °C to that at 4 °C.

Western blot analysis

Western blotting was conducted following a standard protocol. Briefly, protein lysates were extracted from cells and quantified with a BCA assay. The protein samples were separated on 10% gels by SDS–PAGE, transferred to PVDF membranes, blocked with 5% BSA, and incubated with the indicated primary antibodies overnight at 4 °C and then with the appropriate HRP-conjugated secondary antibody. Detection was

performed with a Tanon system (Bio-Rad, Hercules, CA, USA) using a Western ECL kit (Beyotime, Shanghai, China). Densitometric analysis of the gels was performed using ImageJ software.

Immunofluorescence analysis

For cellular immunofluorescence, transfected THP-1 monocytes and BMDMs were seeded onto coverslips in 12-well plates and differentiated into M1 macrophages as described above. The cells were fixed with 4% paraformaldehyde, treated with 0.1% Triton-X-100 and stained with anti-CD68 (1:500 dilution; Abcam, Cambridge, UK) and anti-CD86 (1:400 dilution; Santa Cruz Biotechnology, TX, USA) or with anti-F4/80 (1:500 dilution; CST, Danvers, MA, USA) and anti-CD86 (1:300 dilution; CST, Danvers, MA, USA) at 4 °C overnight. For tissue immunofluorescence, fixed paraffin-embedded mouse spleen tissue sections were subjected to antigen retrieval by Tris-EDTA plus Tween 20 buffer (pH 8.0). The tissue sections were then treated with 3% H_2O_2, blocked with 3% BSA, and incubated with anti-F4/80 (1:500 dilution; CST, Danvers, MA, USA) and anti-CD86 (1:300 dilution; CST, Danvers, MA, USA) antibodies at 4 °C overnight. Subsequently, the slides or tissue sections were incubated with appropriate fluorescence-labeled secondary antibodies (1:500 dilution) at room temperature (RT) for 1 h and then counterstained with DAPI. Images were obtained with an upright fluorescence microscope (NIKON ECLIPSE CI-S, Tokyo, Japan). The level of immunofluorescence intensity of CD86 or CD206, which was defined as the mean gray value, was determined using ImageJ software (https://imagej.net). The mean fluorescence intensity (mean gray value) of the control group was normalized to 1.

Coimmunoprecipitation (co-IP), mass spectrometry (MS), and bioinformatics analyses

Bone marrow-derived M1 macrophages were incubated with IgG-coated latex beads for 2 h at 37 °C. Immunoprecipitation was conducted following the manufacturer's instructions. Briefly, protein A/G beads (MCE, Shanghai, China) were incubated with the antibodies at 4 °C for 2 h. Total protein was extracted from bone marrow-derived M1 macrophages using IP lysis buffer (Beyotime) and quantified with a BCA assay kit (Thermo Fisher). Equal amounts of protein (1000 μg) were incubated with the antibody-bead compounds at 4 °C overnight. The mixture was then washed seven times with IP lysis buffer, suspended in 1× SDS–PAGE loading buffer, boiled at 95 °C for 5 min and analyzed by immunoblot analysis or mass spectrometry detection.

Mass spectrometry (MS) detection was conducted by Shanghai Luming Biotechnology Co., Ltd. (Shanghai, China). Briefly, the MST4- and IgG-bound proteins were resolved in the gel and stained with Coomassie Blue (Beyotime). The gel was then decolorized and digested with trypsin, and acetonitrile was used to obtain the peptides. Data-dependent acquisition mass spectrum techniques were used to acquire tandem MS data with a ThermoFisher Q Exactive mass spectrometer. Proteome Discover 2.5 software was analysed the LC–MS/MS data with the UniProt mouse database (released 6 Dec 2020). In the present study, protein identification was supported by at least one unique peptide in the high-confidence protein.

The interaction proteins of MST4 were predicted based on the average functional similarities between MST4 and its interaction partners as described previously [37]. The semantic similarity in the GO terms of the BP, MF, and CC categories was determined with the GOSemSim package using Wang's method. Based on the semantic similarity scores for GO terms, the functional similarity was designed to assess the strength of the relationship between each protein and its partners by considering functional association or location proximity.

Phosphoproteomics analysis

Four samples from each group were included in the analysis, and MS detection was conducted at Shanghai Luming Biotechnology. Briefly, proteins from M1 macrophages derived from bone marrow cells were collected by scraping, extracted, and quantified using a BCA assay kit. The total proteins were then subjected to enzyme digestion, iTRAQ labeling, and desalting, and the phosphopeptides were enriched with titanium dioxide beads (TiO_2) and analyzed by LC–MS/MS. Database searches of all raw files were processed using ProteinPilot software version 5.0. Trypsin digestion specificity and the cysteine alkylation option were applied in the database searches. Motif analysis was performed with the Modification Motifs tool (http://meme-suite.org/tools/momo) to identify the hypo- and hyperphosphorylation site (hypo-PS and hyper-PS, respectively) motifs. Kinase-substrate enrichment analysis of the phosphoproteomics data was performed using the clusterProfiler package and kinase-substrate "gene sets" assembled from PhosphoSitePlus as described previously [38].

Statistical analysis

All statistical analyses were performed with SPSS 19.0 software for Windows (SPSS, Chicago, IL, USA). The data are expressed as means ± SEMs or medians (95% confidence interval). The normality of the data was assessed by the Kolmogorov–Smirnov test. Student's *t* test and the Wilcoxon rank-sum (Mann–Whitney) test were used for data that followed a normal distribution and those that did not, respectively. For the comparison of multiple groups, one-way ANOVA with the least significant difference test for post-hoc multiple comparisons and the Kruskal–Wallis test were used for data that fulfilled a normal distribution and those that did not, respectively. For all tests, a two-tailed $P < 0.05$ was considered to indicate statistical significance.

RESULTS

Pathological features of M1-like macrophages and MST4 in ITP patients

Using CD14 and CD86 as molecular markers [35], M1-like macrophages were characterized from ITP patients and HCs by flow cytometry. The population of M1-like macrophages was determined to be expanded in newly diagnosed primary ITP patients compared with HCs (10.167% ± 0.884% vs. 5.290% ± 0.392%; $P < 0.001$; Fig. 1A). According to their responses, ITP patients were classified as CR or PR + NR. Before HD-DXM treatment, both CR (CR-pre) and PR + NR (PR + NR-pre) patients showed an increased population of M1-like macrophages (CR: 9.732% ± 1.072% vs. 5.290% ± 0.392%, $P < 0.001$; PR + NR: 11.038% ± 1.605% vs. 5.290% ± 0.392%, $P < 0.001$; Fig. 1B). After HD-DXM treatment, the numbers of M1-like macrophages were decreased (restored back) to a lower level in CR patients (9.732% ± 1.072% vs. 5.910% ± 0.400%; $P < 0.001$; Fig. 1C). No significant difference in the PR + NR patients was observed between before and after treatment (11.038% ± 1.605% vs. 9.785% ± 1.208%; $P > 0.05$; Fig. 1C).

The expression of M1 cytokines, CD80, and IRF5 in M1-like macrophages was examined by qRT-PCR. The mRNA expression levels of *IRF5*, *CD80*, *IL-1β*, *IL-6*, *IL-12*, and *TNF-α* were increased in newly diagnosed ITP patients (Fig. 1D–I). After HD-DXM treatment, the mRNA levels of *IRF5*, *IL-1β*, *IL-6*, and *TNF-α* in CR patients and the mRNA level of *TNF-α* in PR + NR patients were restored to a lower level, whereas the expression of *CD80* and *IL-12* in CR patients and the expression of *IRF5*, *CD80*, *IL-1β*, *IL-6*, and *IL-12* in PR + NR patients did not significantly change (Fig. 1D–I).

The expression of MST4 in M1 macrophages increased significantly in newly diagnosed primary ITP patients (Fig. 1J, Supplementary Fig. 4A). After HD-DXM treatment, the expression of MST4 in M1 macrophages remained higher in ITP patients than in HCs (Supplementary Fig. 4B), whereas decreased expression of MST4 after HD-DXM treatment was observed in CR patients (Fig. 1K, Supplementary Fig. 4A, B); however, treatment did not significantly change the expression of *MST4* in PR + NR patients (Fig. 1K, Supplementary Fig. 4A, B). The mRNA level of *Mst4* in splenic macrophages was further determined in a murine passive ITP model. The results showed that the expression of *Mst4* was increased in ITP mice (Supplementary Fig. 4C). A significant positive correlation between the expression of *MST4* and the expression of *IRF5* was observed in newly diagnosed ITP patients (Fig. 1L), especially in CR-pre patients (Fig. 1M). No such association was found in the PR + NR-pre group (Fig. 1N).

MST4 is upregulated in THP-1-derived M1 macrophages

To determine the role of MST4 in the development of M1 macrophages, THP-1 human monocytic cells were induced to differentiate into M1 macrophages by LPS + IFN-γ and collected at multiple time points. The mRNA expression levels of *STAT1* and

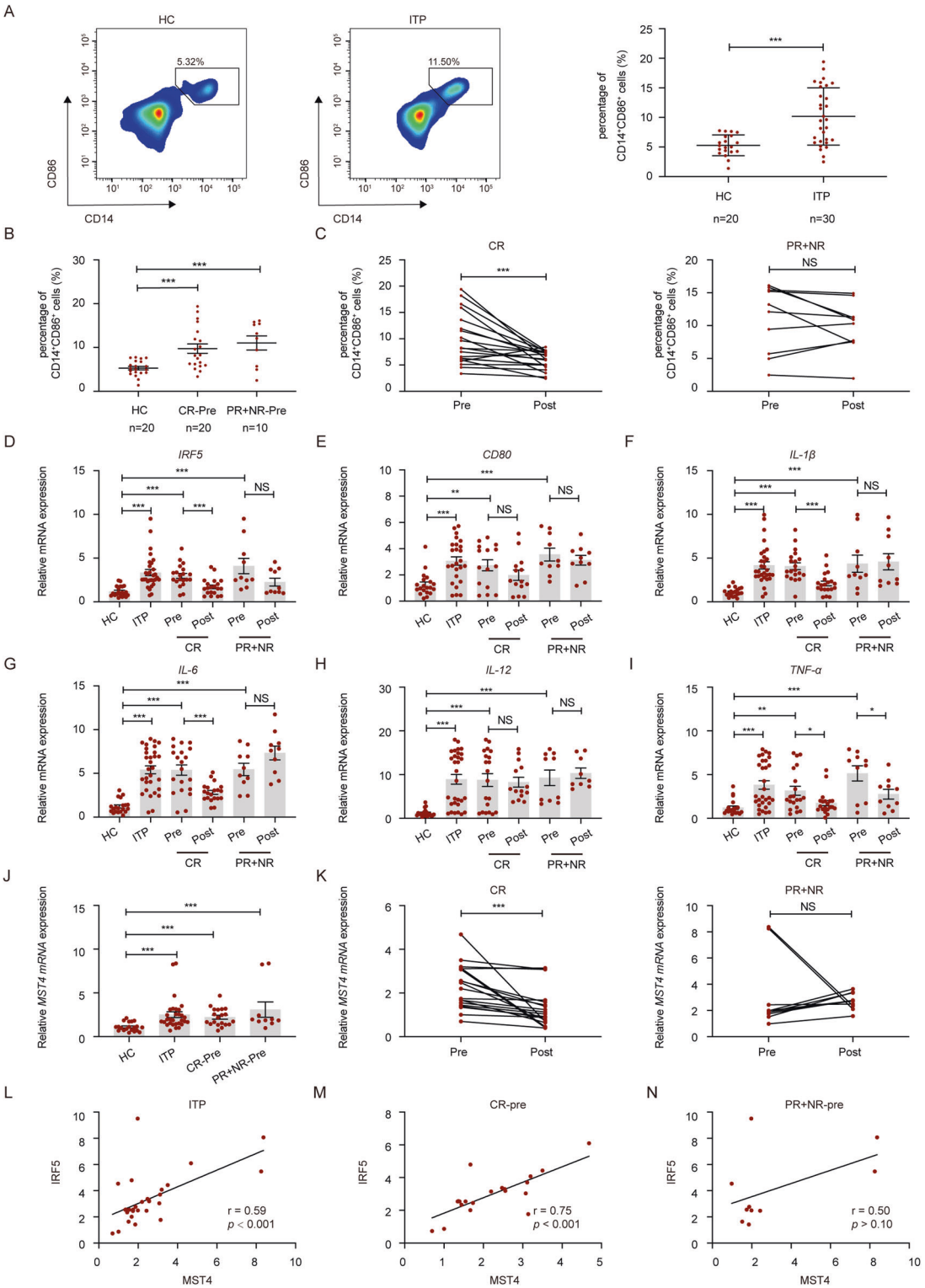

Fig. 1 M1 macrophages and expression of *IRF5, CD80, IL-1β, IL-6, IL-12, TNF-a*, and *MST4* in M1 macrophages of ITP patients. **A**–**C** Representative flow cytometry plots of $CD14^{+}CD86^{+}$ M1-like macrophages. The peripheral $CD14^{+}CD86^{+}$ M1-like macrophage population was expanded in ITP patients and restored to a lower level by the HD-DXM regimen in CR patients. **D**–**I** In magnetically isolated $CD14^{+}$ cells, the expression of *IRF5*, *CD80*, *IL-1β*, *IL-6*, *IL-12*, and *TNF-a* was increased in ITP patients, and the expression of *IRF5*, *IL-1β*, *IL-6*, and *TNF-a* was restored to a lower level by the HD-DXM regimen in CR patients. **J**, **K** The expression of *MST4* in M1 macrophages was enhanced in ITP patients and was restored to a lower level by the HD-DXM regimen in CR patients. **L**–**N** A positive correlation between *MST4* and *IRF5* was found in ITP patients ($r = 0.59$, $p < 0.001$), especially in CR-pre patients ($r = 0.75$, $p < 0.001$). The data are presented as the means ± SEMs in all the panels. *P* values were calculated using unpaired Student's *t* test (**A**, **B**, **D**–**J**), paired Student's *t* test (**C**, **K**), or Spearman's correlation analysis (**L**–**N**). $^{*}p < 0.05$, $^{**}p < 0.01$, $^{***}p < 0.001$. ITP, primary immune thrombocytopenia; HC healthy control, pre before treatment, post after treatment, HD-DXM high-dose dexamethasone, CR complete response, PR partial response, NR no response, NS no significance

IRF5 were increased after stimulation and peaked at 24 h, indicating the successful induction of M1 macrophages (Fig. 2A). During LPS + IFN-γ stimulation, the expression of *MST4* increased gradually, peaked at 16 h and then decreased (Fig. 2A). Consistent with our previous study [30], the protein level of MST4 was reduced during the first 4 hours and subsequently upregulated during the development of M1 macrophages (Fig. 2B, Supplementary Fig. 5A).

MST4 regulates the phagocytic capacity and M1 macrophage polarization

To determine the specific role of MST4 in modulating the function of M1 macrophages, THP-1 cells were transfected with a lentiviral vector containing MST4-specific shRNA for the knockdown of *MST4* (sh-MST4 group), cDNA of human *MST4* for the overexpression of *MST4* (OE group), control shRNA with a scrambled sequence (sh-Scr group) or an empty vector, and the cells were then induced to differentiate into macrophages as described above. In the absence of LPS + IFN-γ stimulation, the numbers of $CD86^+$ macrophages and the mRNA levels of *CD80*, CD86, *IRF5, STAT1, TNF-α, IL-12*, and *iNOS* in macrophages were not modulated by MST4 (Supplementary Fig. 5B–E). The mRNA level of *IL-1β* was decreased in macrophages of the sh-MST4 group, and the mRNA level of *IL-6* was increased in macrophages of the OE group (Supplementary Fig. 5E). In the presence of LPS + IFNγ stimulation, the expression levels of CD86, CD80 and the M1 transcription factor *IRF5* in M1 macrophages were decreased in the sh-MST4 group and increased in the OE group (Supplemental Fig. 6A–C), whereas the mRNA expression level of *STAT1* was not regulated by MST4 (Supplemental Fig. 6D). Consistently, M1 macrophages of the sh-MST4 group showed a reduced signal intensity of CD86 compared with the sh-Scr group, as revealed by the immunofluorescence analysis (Fig. 2C, Supplementary Fig. 6E). Enhanced signal intensity of CD86 was observed in M1 macrophages of the OE group (Fig. 2C, Supplementary Fig. 6F). The mean fluorescence intensity (MFI) of CD86 in M1 macrophages was decreased in the sh-MST4 group but increased in the OE group (Fig. 2D). Although the mRNA levels of *IL-12* and *iNOS* were not modulated by MST4 (Supplementary Fig. 6G, H), the mRNA expression levels of *IL-1β*, *IL-6*, and *TNF-α* in M1 macrophages were decreased in the sh-MST4 group but increased in the OE group (Fig. 2E).

To evaluate whether MST4 regulates FcγR-mediated phagocytosis, M1 macrophages induced from transfected THP-1 cells were incubated with IgG-coated latex beads for 2 h. As shown in Fig. 2F, the phagocytosis of IgG-coated latex beads by M1 macrophages was inhibited by blocking FcγRs. Without blocking FcγRs, the number of IgG-coated latex beads internalized by M1 macrophages was decreased in the sh-MST4 group and increased in the OE group (Fig. 2F). Moreover, M1 macrophages in the sh-MST4 group showed a significantly compromised phagocytic index compared with the sh-Scr group, whereas the M1 macrophages in the OE group exhibited an increased phagocytic index (Fig. 2G). Furthermore, the mRNA expression level of *FcγRs* in M1 macrophages without stimulation with IgG-coated latex beads was determined. Despite the reduced expression levels of *FcγRIIa*, *FcγRIIb*, and *FcγRIII*, *FcγRIIb* dominated in M1 macrophages of the sh-MST4 group due to a reduced *FcγRIIa/FcγRIIb* ratio at the mRNA level (Fig. 2H–I). In contrast, M1 macrophages of the OE group showed increased expression levels of *FcγRIIa*, *FcγRIIb*, and *FcγRIII*, and *FcγRIIa* dominated due to an increased *FcγRIIa/FcγRIIb* mRNA ratio (Fig. 2H–I). Moreover, the expression of *FcγRI* in M1 macrophages was not affected by MST4 (Fig. 2H).

Genetic ablation of Mst4 in macrophages ameliorates thrombocytopenia in mice

To explore the potential role of MST4 in the pathogenesis of ITP in vivo, we generated mice with macrophage-specific knockout of *Mst4* ($Mst4^{\Delta M/\Delta M}$) by crossbreeding $Mst4^{fl/fl}$ mice with LyzM-Cre mice. A passive murine ITP model was induced by an anti-platelet monoclonal antibody (Fig. 3A). The ablation of *Mst4* in macrophages alleviated thrombocytopenia in the $Mst4^{\Delta M/\Delta M}$ ITP model (Fig. 3B). Moreover, a decreased number of M1 macrophages (Fig. 3C, Supplementary Fig. 7A) and an increased number of M2 macrophages (Fig. 3D, Supplementary Fig. 7B) in splenocytes were observed in the $Mst4^{\Delta M/\Delta M}$ ITP model, as revealed by immunofluorescence analysis.

RNA-seq analysis was employed to assess the global gene expression profiles of macrophages in $Mst4^{fl/fl}$ ITP mice and $Mst4^{\Delta M/\Delta M}$ ITP mice ($n = 4$, female). A total of 279 genes were differentially expressed (152 upregulated and 127 downregulated genes in splenic macrophages of the $Mst4^{\Delta M/\Delta M}$ ITP mice compared with the $Mst4^{fl/fl}$ ITP mice) (Fig. 3E, Supplementary Table 3). According to the KEGG analysis and GSEA results, various pathways associated with inflammation and phagocytosis, including the NF-κB-, MAPK-, JAK-STAT-, and FcγR-mediated phagocytosis pathways, were enriched (Fig. 3F, G, Supplementary Table 4). Immunoblotting analysis showed compromised activation of the JAK2/STAT1, NF-κB, MAPK and FcγR-mediated phagocytosis pathways in macrophages of $Mst4^{\Delta M/\Delta M}$ ITP mice (Fig. 3H) and sh-MST4 macrophages (Supplementary Fig. 7D), indicating compromised M1 polarization of macrophages in the absence of MST4. These signaling pathways were relatively active in macrophages of the OE group (Supplemental Fig. 7E).

M1 polarization of macrophages is suppressed in $Mst4^{\Delta M/\Delta M}$ passive ITP mice

No significant differences in the baseline levels of M1 and M2 macrophages in the spleen (Supplementary Fig. 8A, B) and peritoneal lavage fluid (Supplementary Fig. 8C, D) were found between the $Mst4^{\Delta M/\Delta M}$ mice and the $Mst4^{fl/fl}$ mice prior to the induction of ITP. As shown in Fig. 4A–D, M1 macrophages were attenuated, whereas M2 macrophages expanded and dominated in the spleen and peritoneal lavage fluid of $Mst4^{\Delta M/\Delta M}$ ITP mice. Consistent with these results, the mRNA expression levels of M1 cytokines (*Il-1β*, *Il-6*, *Il-12*, and *Tnf-α*) were decreased in macrophages purified from splenocytes of $Mst4^{\Delta M/\Delta M}$ ITP mice (Fig. 4E).

Subsequently, the protein levels of FcγRs, including FcγRI, FcγRIIb, and FcγRIII, in splenic macrophages of ITP mice were determined by flow cytometry. Representative flow cytometer plots are shown in Fig. 4F. The MFIs of FcγRI, FcγRIIb, and FcγRIII in macrophages of $Mst4^{\Delta M/\Delta M}$ ITP mice were higher than those in the $Mst4^{fl/fl}$ ITP mice (Fig. 4G). Notably, the inhibitory FcγRIIb dominated in macrophages of $Mst4^{\Delta M/\Delta M}$ ITP mice, as reflected by increased FcγRIIb/FcγRI and FcγRIIb/FcγRIII ratios (Fig. 4H).

The phagocytic capacity of M1 macrophages from $Mst4^{\Delta M/\Delta M}$ ITP mice is compromised

To further determine the effects of MST4 on the development and function of M1 macrophages in ITP mice, bone marrow cells were isolated and induced into M1 macrophages by LPS + IFNγ. A compromised signal intensity of the M1 marker CD86 and a decreased number of M1 macrophages were observed in $Mst4^{\Delta M/\Delta M}$ ITP mice (Fig. 5A, B). Consistent with these findings, relatively lower mRNA expression levels of *Il-1β, Il-6, Tnf-α, inos*, and *Il-12* were observed in these M1 macrophages of $Mst4^{\Delta M/\Delta M}$ ITP mice (Fig. 5C).

To determine the phagocytic capacity, M1 macrophages of $Mst4^{\Delta M/\Delta M}$ ITP mice or $Mst4^{fl/fl}$ ITP mice were incubated with antibody-opsonized platelets for 2 h. As shown in Supplementary Fig. 9A, the phagocytosis of antibody-opsonized platelets by M1 macrophages was inhibited by FcγR blockade. The number of internalized antibody-opsonized platelets and the phagocytic index were found to be significantly decreased in M1 macrophages of $Mst4^{\Delta M/\Delta M}$ ITP mice compared with those of $Mst4^{fl/fl}$ ITP mice (Fig. 5D–F). Despite considerably decreased protein levels of FcγRI, FcγRIIb, and FcγRIII in M1 macrophages of $Mst4^{\Delta M/\Delta M}$ ITP mice (Fig. 5G, Supplementary Fig. 9B), FcγRIIb

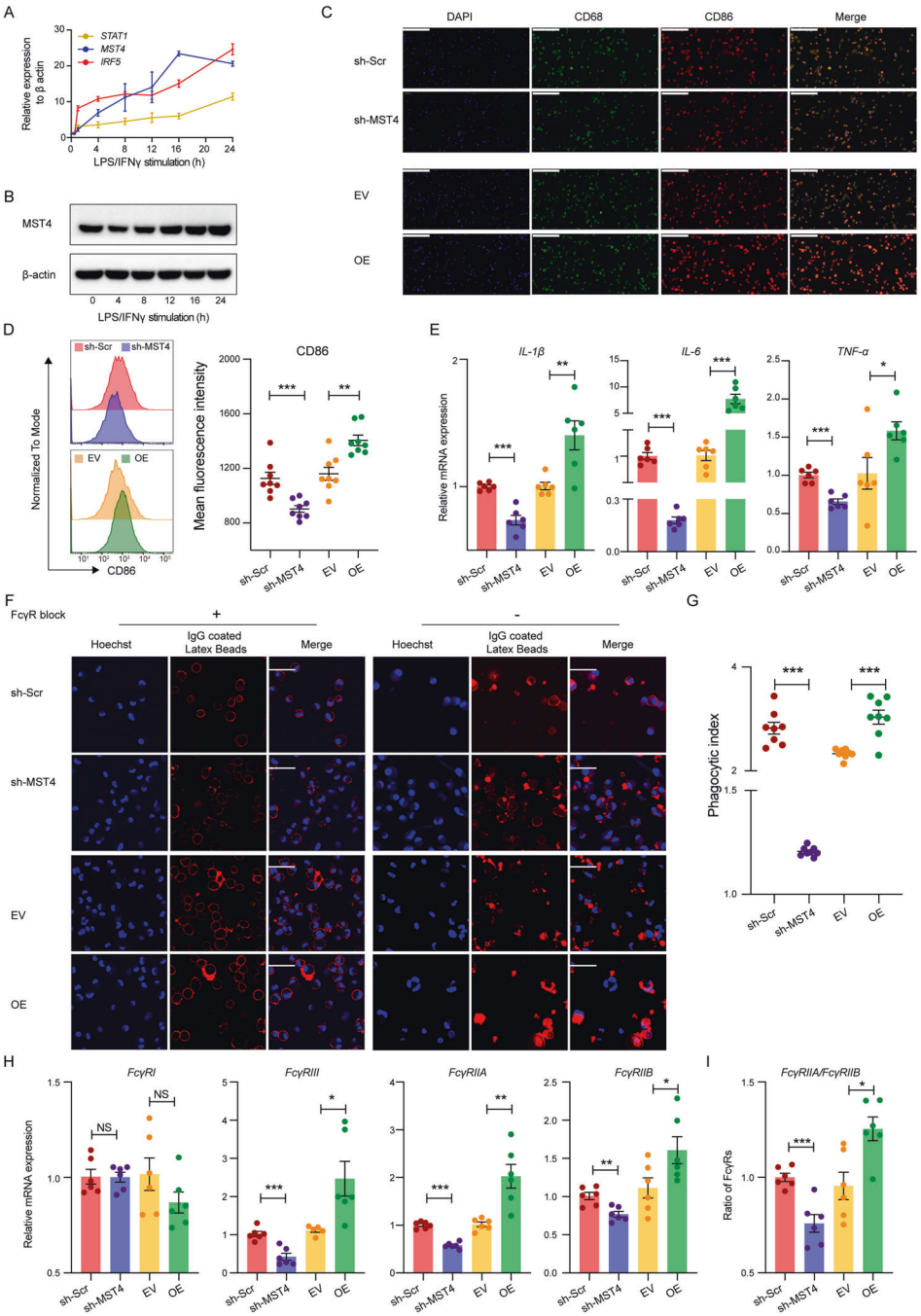

Fig. 2 MST4 kinase promotes the phagocytic capacity of M1 macrophages derived from THP-1 monocytes. THP-1 monocytes were stimulated with LPS + IFN-γ and collected at multiple time points. The expression of MST4 during the development of M1 macrophages was determined by qRT–PCR (**A**) and immunoblot analysis (**B**). THP1 monocytes were transduced with lentivirus containing MST4-shRNA, control shRNA, cDNA of human MST4, or empty vector and were polarized into M1 macrophages by incubation with LPS + IFN-γ for 24 h. **C** Representative immunostaining images of M1 macrophages. Original magnification, ×200. Scale bar, 200 μm. **D** Representative FACS histogram plot of CD86 (left) and MFI quantification of CD86 in M1 macrophages (right). **E** The expression of *IL-1β*, *IL-6*, and *TNF-α* was decreased in M1 macrophages of the sh-MST4 group and increased in M1 macrophages of the OE group. M1 macrophages induced from THP-1 cells were incubated with IgG-coated latex beads for 2 h. **F** The phagocytosis of IgG-coated latex beads by M1 macrophages was compromised by blocking FcγRs (left), and the number of endocytic IgG-coated latex beads in M1 macrophages was decreased in the sh-MST4 group and increased in the OE group (right). Original magnification, ×400. Scale bar, 50 μm. **G** The phagocytic index (the ratio of IgG-coated latex bead-positive macrophages at 37 °C to that at 4 °C) was reduced in the sh-MST4 group and increased in the OE group, as revealed by a FACS analysis. **H–I** The expression of *FcγRI* was not regulated by MST4. The expression of *FcγRIIa*, *FcγRIIb*, and *FcγRIII* was decreased in M1 macrophages of the sh-MST4 group, and *FcγRIIb* dominated. In M1 macrophages of the OE group, the expression of *FcγRIIa*, *FcγRIIb*, and *FcγRIII* was increased, and *FcγRIIa* dominated. The data are presented as the means ± SEMs in all the panels. *P* values were calculated using unpaired Student's *t* test (**D**, **E**, **G**, **H**, **I**). *$p < 0.05$, **$p < 0.01$, ***$p < 0.001$. NS no significance, sh-MST4 *MST4*-specific short hairpin RNA, sh-Scr control shRNA with a scrambled sequence, EV empty vector, OE overexpression

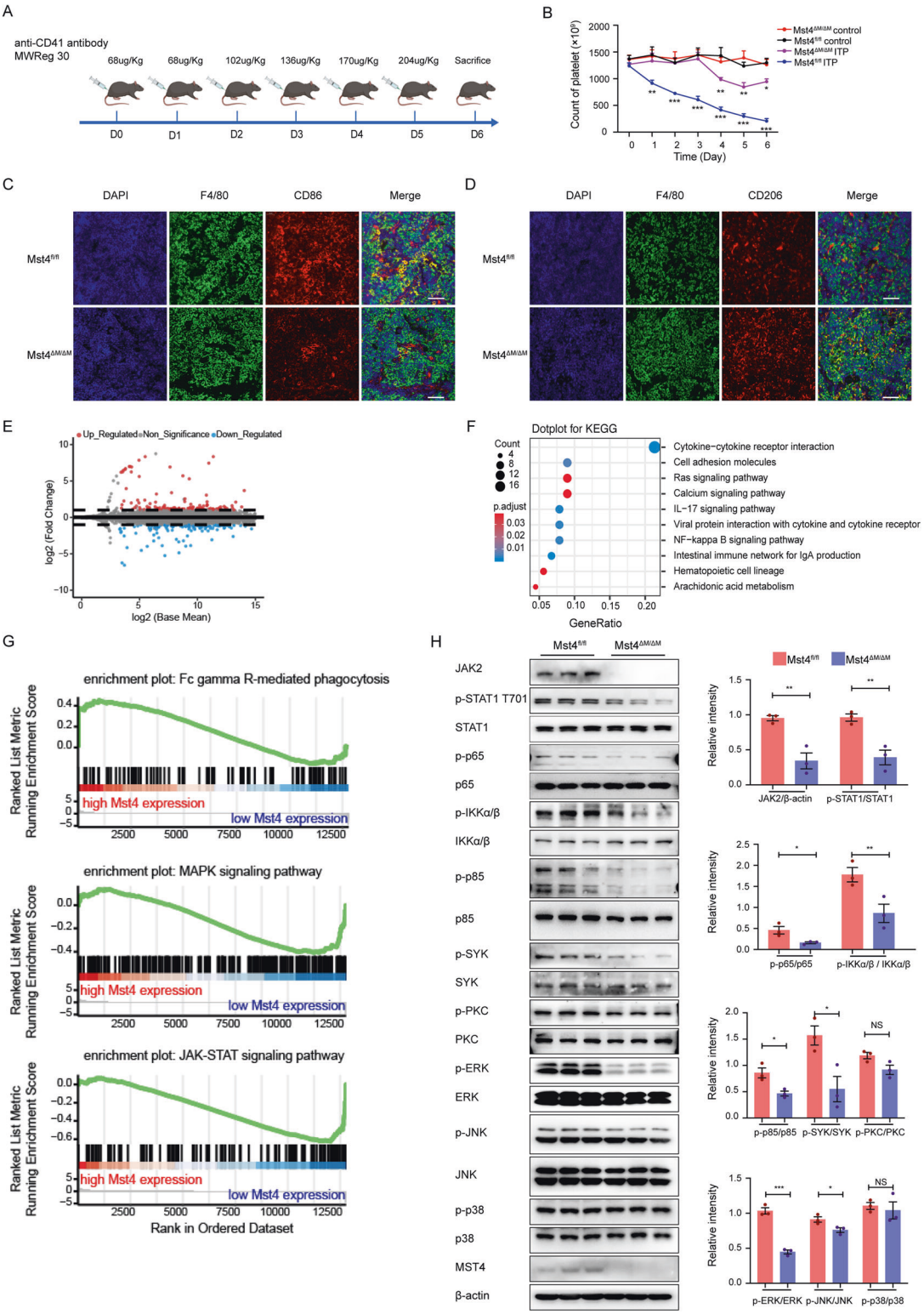

Fig. 3 MST4 deficiency in macrophages ameliorates thrombocytopenia in the passive murine ITP model. **A** Schematic of the murine passive ITP model. **B** Thrombocytopenia was ameliorated in $Mst4^{\Delta M/\Delta M}$ ITP mice. **C**, **D** Representative immunofluorescence images of M1 and M2 macrophages in spleens of $Mst4^{\Delta M/\Delta M}$ and $Mst4^{fl/fl}$ ITP mice. Original magnification, ×400. Scale bar, 50 μm. **E** MA plot of differentially expressed genes in splenic macrophages between $Mst4^{fl/fl}$ and $Mst4^{\Delta M/\Delta M}$ ITP mice ($n = 4$). The NF-κB pathways, JAK-STAT pathways, MAPK pathways, and FcγR-mediated phagocytosis were differently activated between $Mst4^{\Delta M/\Delta M}$ and $Mst4^{fl/fl}$ ITP mice, as revealed by KEGG (**F**) and gene set enrichment analyses (**G**). **H** Immunoblot analysis of the characterized proteins of the JAK-STAT (JAK2, STAT1(Tyr701)) pathway, FcγR-mediated phagocytosis (SYK, p85, PKC), NF-κB (Ikkα/β, NF-κB (p65)) pathway, and MAPK (ERK, JNK, p38) pathway in M1 macrophages of $Mst4^{\Delta M/\Delta M}$ and $Mst4^{fl/fl}$ ITP mice (left). The relative intensity (phosphorylated proteins relative to total protein or total protein relative to β-actin) is shown (right). β-actin was used as the loading control. The data are presented as the means ± SEMs in all the panels. $^{*}p < 0.05$, $^{**}p < 0.01$, $^{***}p < 0.001$

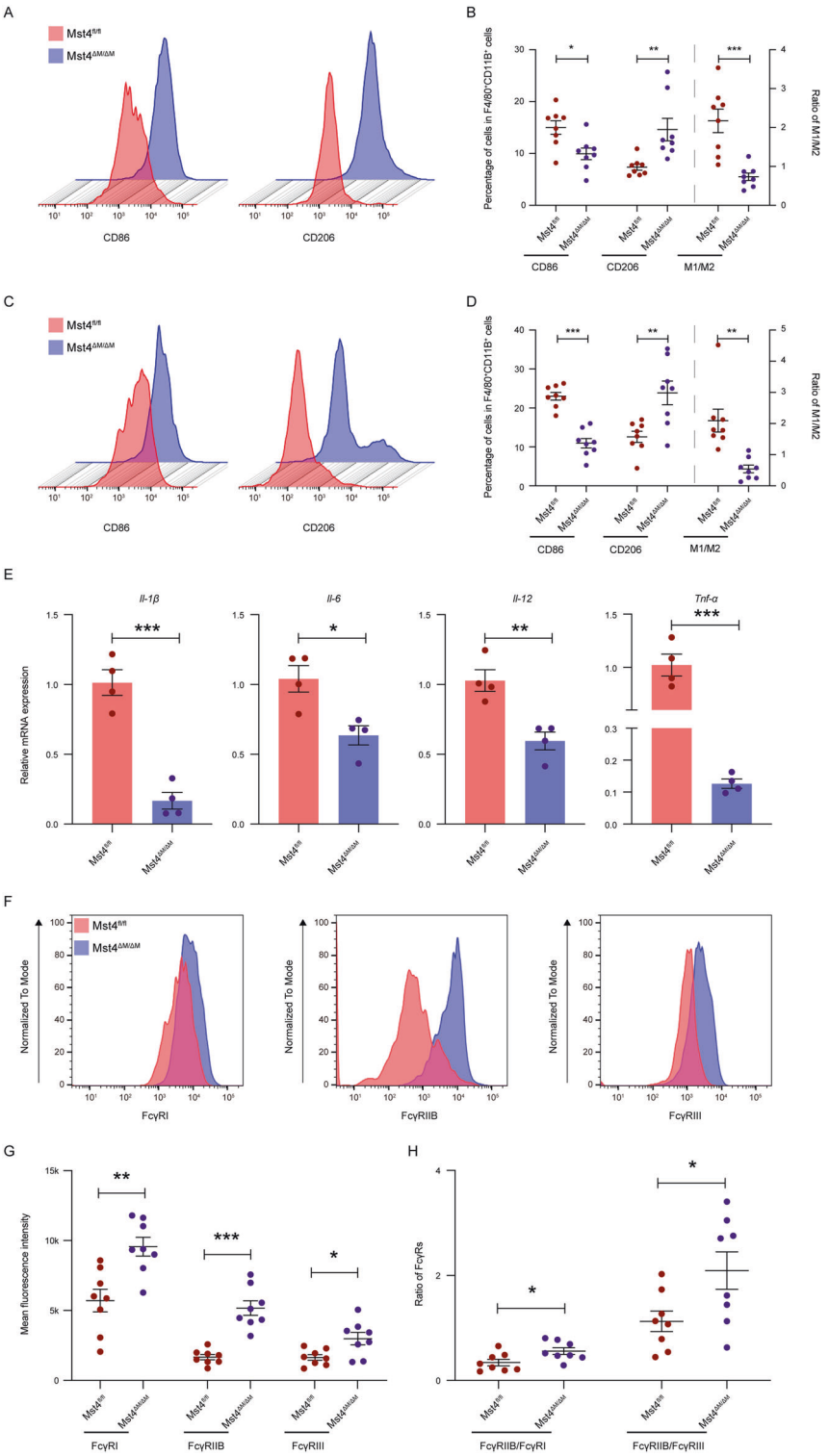

Fig. 4 The M1 macrophage population and expression of FcγRs in macrophages are attenuated in *Mst4*$^{\Delta M/\Delta M}$ ITP mice. **A** Representative FACS histogram plots of CD86 (left) and CD206 (right) in F4/80^{+}CD11B^{+} splenocytes of *Mst4*$^{\Delta M/\Delta M}$ and *Mst4*$^{fl/fl}$ ITP mice. **B** A decreased number of M1 macrophages, an expanded population of M2 macrophages, and a predominance of M2 macrophages in F4/80^{+}CD11B^{+} splenic macrophages were observed in *Mst4*$^{\Delta M/\Delta M}$ ITP mice. **C** Representative FACS histogram plot of CD86 (left) and CD206 (right) in F4/80^{+}CD11B^{+} cells of peritoneal lavage fluid from *Mst4*$^{\Delta M/\Delta M}$ and *Mst4*$^{fl/fl}$ ITP mice. **D** A decreased number of M1 macrophages, an expanded population of M2 macrophages, and a predominance of M2 macrophages in F4/80^{+}CD11B^{+} cells were observed in the peritoneal lavage fluid of *Mst4*$^{\Delta M/\Delta M}$ ITP mice. **E** The expression of *Il-1β*, *Il-6*, *Il-12*, and *Tnf-α* was decreased significantly in magnetically sorted F4/80^{+} splenic macrophages of *Mst4*$^{\Delta M/\Delta M}$ ITP mice. **F** Representative FACS histogram plots of FcγRI, FcγRIIb, and FcγRIII in F4/80^{+}CD11B^{+} splenic macrophages of *Mst4*$^{\Delta M/\Delta M}$ and *Mst4*$^{fl/fl}$ ITP mice. F4/80^{+}CD11B^{+} splenic macrophages of *Mst4*$^{\Delta M/\Delta M}$ ITP mice showed enhanced expression of FcγRI, FcγRIIb, and FcγRIII (**G**) and a predominance of FcγRIIb (**H**). The data are presented as the means ± SEMs in all the panels. *$p < 0.05$, **$p < 0.01$, ***$p < 0.001$. MFI mean fluorescence intensity

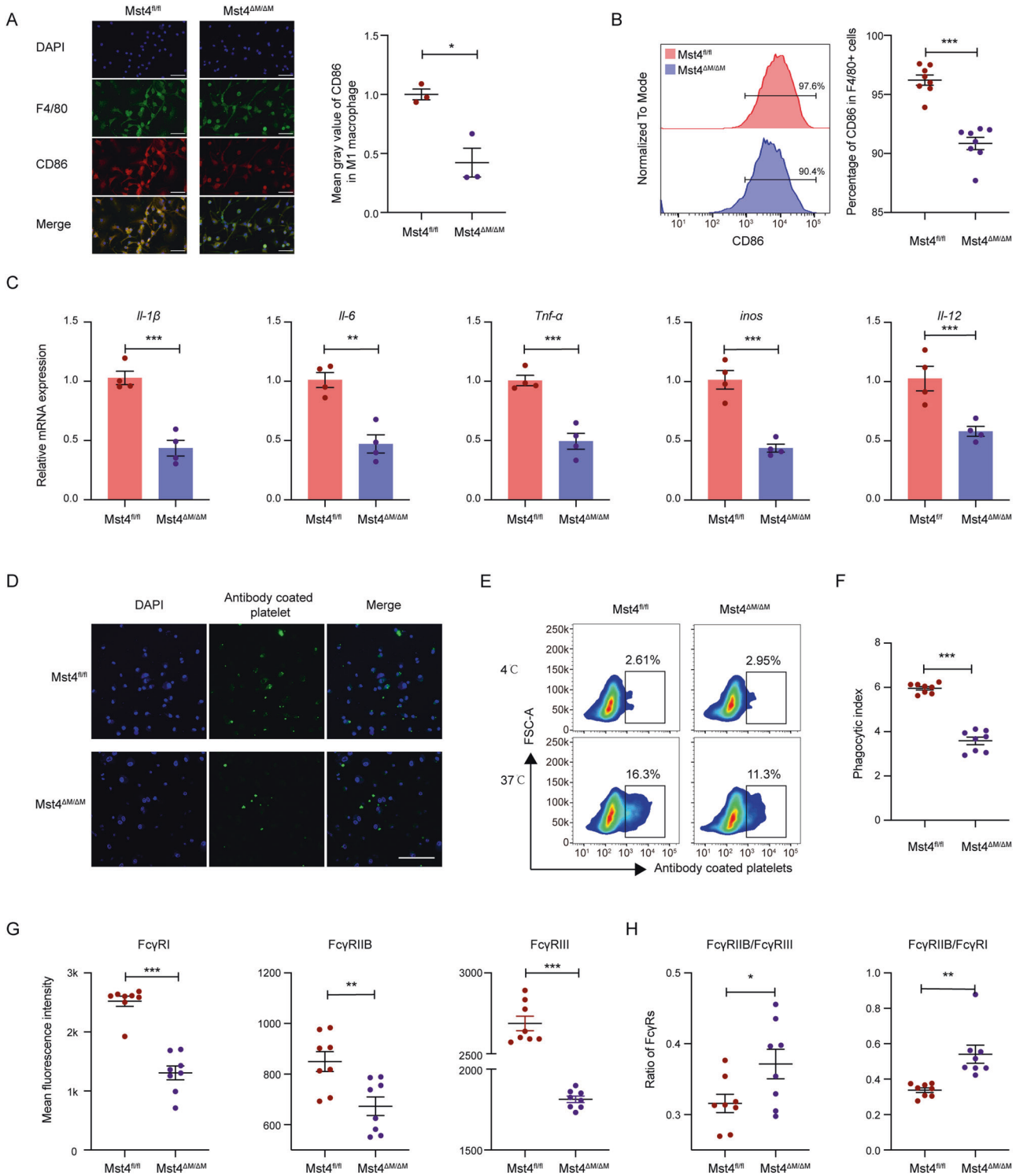

Fig. 5 The development and phagocytic capacity of M1 macrophages derived from BMDMs of *Mst4*$^{\Delta M/\Delta M}$ ITP mice are compromised. Bone marrow-derived macrophages (BMDMs) of *Mst4*$^{\Delta M/\Delta M}$ and *Mst4*$^{fl/fl}$ ITP mice were stimulated with LPS + IFN-γ for 24 h to generate M1 macrophages. **A** Representative immunostaining images of M1 macrophages (left). Original magnification, ×400. Scale bar, 50 μm. The quantification of the immunofluorescence intensity of CD86 (mean gray value) is shown. The mean gray value of the control group was normalized to 1 (right). **B** Representative FACS histogram of CD86 (left) and percentage of CD86 in M1 macrophages (right). **C** The expression of *Il-1β*, *Il-6*, *Tnf-α*, *iNOS*, and *Il-12* was reduced in M1 macrophages of *Mst4*$^{\Delta M/\Delta M}$ ITP mice. **D**–**F** M1 macrophages of *Mst4*$^{\Delta M/\Delta M}$ and *Mst4*$^{fl/fl}$ ITP mice were incubated with antibody-opsonized platelets for 2 h. Representative immunofluorescence staining of the phagocytosis assay without FcγR blocking was performed. Original magnification, ×400. Scale bar, 100 μm (**D**). Representative flow cytometry plots of the phagocytosis assay (**E**), and the phagocytic index was reduced in M1 macrophages of *Mst4*$^{\Delta M/\Delta M}$ ITP mice (**F**). M1 macrophages of *Mst4*$^{\Delta M/\Delta M}$ ITP mice showed decreased expression of FcγRI, FcγRIIb, and FcγRIII (**G**), and FcγRIIb dominated (**H**), as revealed by FACS analysis. The data are presented as the means ± SEMs in all the panels. *$p < 0.05$, **$p < 0.01$, ***$p < 0.001$. MFI mean fluorescence intensity

appeared to be the dominant FcγR, as shown by markedly increased FcγRIIb/FcγRI and FcγRIIb/FcγRIII ratios in M1 macrophages of $Mst4^{\Delta M/\Delta M}$ ITP mice compared with those of $Mst4^{fl/fl}$ ITP mice (Fig. 5H).

MST4 promotes M1 polarization of macrophages by phosphorylating STAT1

To dissect the molecular mechanisms through which MST4 regulates ITP, bone marrow-derived M1 macrophages were incubated with IgG-coated latex beads for 2 h. Subsequently, an MST4 antibody was used to pull down endogenous MST4 protein from extracts of M1 macrophages for mass spectrometry analysis. Candidate binding partners of MST4 were identified according to functional similarities [37]. Figure 6A summarizes the distributions of functional similarities. The lower and upper box boundaries represent the 25th and 75th percentiles, and the line in the box represents the median. The dashed line represents the cutoff value. Proteins with a higher average functional similarity (median value > 0.4) were considered central proteins within the MST4 interactome in M1 macrophages. Among these proteins, STAT1, STAT2, and STAT3 displayed high average functional similarity. Because STAT1 has been demonstrated to be a key transcription factor in M1 macrophages [39], we hypothesized that STAT1 may be involved in ITP as a binding partner of MST4. Because MST4 is a serine/threonine kinase, we also performed phosphoproteomic analysis, which revealed a total of 729 differentially phosphorylated sites between M1 macrophages of $Mst4^{\Delta M/\Delta M}$ ITP mice and those of $Mst4^{fl/fl}$ ITP mice. M1 macrophages of $Mst4^{\Delta M/\Delta M}$ ITP mice displayed 264 hyperphosphorylated sites and 465 hypophosphorylated sites compared with M1 macrophages of $Mst4^{fl/fl}$ ITP mice (Fig. 6B). The kinase-substrate enrichment analysis using the phosphoproteomics data revealed that the JAK-STAT pathway was enriched (Fig. 6C). Protein motif analysis summarized the regular trend of amino acid sequences near phosphorylation sites to speculate the possible pattern in the regions of modification sites (Fig. 6D, Supplementary Fig. 10A–D). The consensus motif PxSP was the most common substrate recognition motif of MST4 (Fig. 6D). Accordingly, the phosphorylation of STAT1 at Ser727 conformed to the most common pattern (Fig. 6E) and was enriched in M1 macrophages from $Mst4^{f/f}$ ITP mice (Fig. 6F). The interaction between MST4 and STAT1 was confirmed by reciprocal coimmunoprecipitation assays of bone marrow-derived M1 macrophages stimulated with IgG-coated latex beads (Fig. 6G±H). Notably, the phosphorylation of STAT1 at Ser727 was reduced in M1 macrophages of $Mst4^{\Delta M/\Delta M}$ ITP mice (Fig. 6I).

The expression of STAT1 in M1 macrophages induced from the magnetically sorted $CD14^+$ monocytes of ITP patients and healthy volunteers was further determined. As shown in Fig. 7A, the phosphorylation of STAT1 at Ser727 and Tyr701 in M1 macrophages was enhanced in ITP patients. HD-DXM treatment reduced the phosphorylation of STAT1 at Ser727 to the normal levels in CR patients, whereas no significant difference in the phosphorylation of STAT1 at both Ser727 and Tyr701 was found between ITP patients and PR + NR-post patients. To further verify the involvement of STAT1 in mediating the MST4-promoted M1 polarization of macrophages in ITP, an activator (2-(1,8-naphthyridin-2-ly) phenol, 2-NP, 50 μM) or inhibitor (fludarabine, 10 μM) of STAT1 was applied to modulate STAT1 expression in LPS/IFNγ-stimulated macrophages. The results showed that the decreased number of M1 macrophages induced in $Mst4^{\Delta M/\Delta M}$ ITP mice could be rescued by 2-NP (Fig. 7B). Consistently, the compromised MFI of CD86 in M1 macrophages of the sh-MST4 group and the enhanced MFI of CD86 in M1 macrophages of the OE group could be reverted by 2-NP and fludarabine, respectively (Supplementary Fig. 11A, B). The relatively lower mRNA expression levels of *Il-1β*, *Il-6*, and *Tnf-α* in M1 macrophages of $Mst4^{\Delta M/\Delta M}$ ITP mice were restored to the normal levels (Fig. 7C). As shown in Supplementary Fig. 11C, D, the compromised and enhanced expression of *IL-1β*, *IL-6*, and *TNF-α* in M1 macrophages of the sh-MST4 and OE groups could be rescued by 2-NP and fludarabine, respectively. Taken together, these results support the notion that MST4 promotes M1 polarization of macrophages in ITP via STAT1 signaling.

DISCUSSION

To the best of our knowledge, this is the first report of elevated levels of *MST4* expression in M1 macrophages of patients with ITP. The present study showed that MST4 positively regulated M1 polarization of macrophages and their FcγR-mediated phagocytosis through phosphorylation of STAT1 and, therefore ameliorated thrombocytopenia in $Mst4^{\Delta M/\Delta M}$ ITP mice. These findings provide convincing evidence for the function and mechanism of MST4 in regulating M1 macrophages in ITP and shed light on novel therapeutic approaches targeting ITP.

ITP patients exhibit decreased platelet production and increased platelet destruction [40–43]. ITP is an autoimmune hemorrhagic disease in which platelets are opsonized by autoantibodies and destroyed primarily by splenic macrophages [1, 41, 44, 45]. Feng et al. [18] illustrated a preferred polarization of M1 macrophages in ITP patients. Consistently, an expansion of circulating M1 macrophages was observed in ITP patients and was restored by glucocorticoids. As the first-line treatment for ITP, glucocorticoids can suppress the synthesis of inflammatory cytokines to exert immunosuppressive effects [46, 47].

MST4 has been implicated in diverse physiological processes and diseases. The expression of MST4 is dysregulated in various diseases, including severe nonalcoholic fatty liver disease, *Aspergillus fumigatus* keratitis, and sepsis [30, 31, 48]. In the current study, enhanced expression of MST4 in circulating M1-like macrophages and a significant correlation between *MST4* and *IRF5* were observed in ITP patients, indicating the involvement of MST4 in the differentiation of M1 macrophages. Ablation of MST4 in M1 macrophages compromised the expression of M1 markers and M1 cytokines. Consistently, attenuated M1 macrophage populations and compromised expression of M1 cytokines in macrophages were found in $Mst4^{\Delta M/\Delta M}$ ITP mice. The depletion of MST4 in macrophages impaired M1 activation upon stimulation with LPS + IFNγ or the IgG-platelet complex, likely by inhibiting the phosphorylation of STAT1. STAT1 can be activated by activating FcγRs, TNF-α, and IFN-γ and is phosphorylated at both Tyr701 and Ser727 for full activation [49, 50]. In the current study, the depletion of MST4 attenuated the phosphorylation of STAT1 at both Tyr701 and Ser727, which in turn compromised the activation and function of M1 macrophages. As one of the major consequences, the expression of proinflammatory cytokines (IL-1β, IL-6, and TNF-α) was reduced in MST4-knockdown M1 macrophages. Consistent with previous studies linking proinflammatory cytokines with the MAPK and NF-κB signaling pathways [51–53], impaired activation of these pathways was also observed in MST4-knockdown M1 macrophages. STAT1 and IRF5 are both important in the polarization of M1 macrophages [54]. Previous studies proved that STAT1 plays critical roles [39, 55]. According to the results of our pilot study, IRF5 was selected as an alternative to study the potential role of MST4 in the development of M1 macrophages in ITP patients.

The amelioration of thrombocytopenia in $Mst4^{\Delta M/\Delta M}$ ITP mice was attributed to their reduced number of splenic M1 macrophages and their compromised phagocytic capacity, which was also reflected by reduced endocytosis of the antibody-platelet complex in MST4-knockdown M1 macrophages. Liu and colleagues demonstrated a disturbed balance between inhibitory and activating FcγRs in ITP patients [24], and this imbalance could be rectified by glucocorticoids, intravenous immunoglobulin, and thrombopoietin receptor agonists [24, 25, 56]. Panchanathan and colleagues demonstrated enhanced expression of FcγRIIb in *Stat1*-deficient splenic cells [57]. In this regard, the attenuated activation

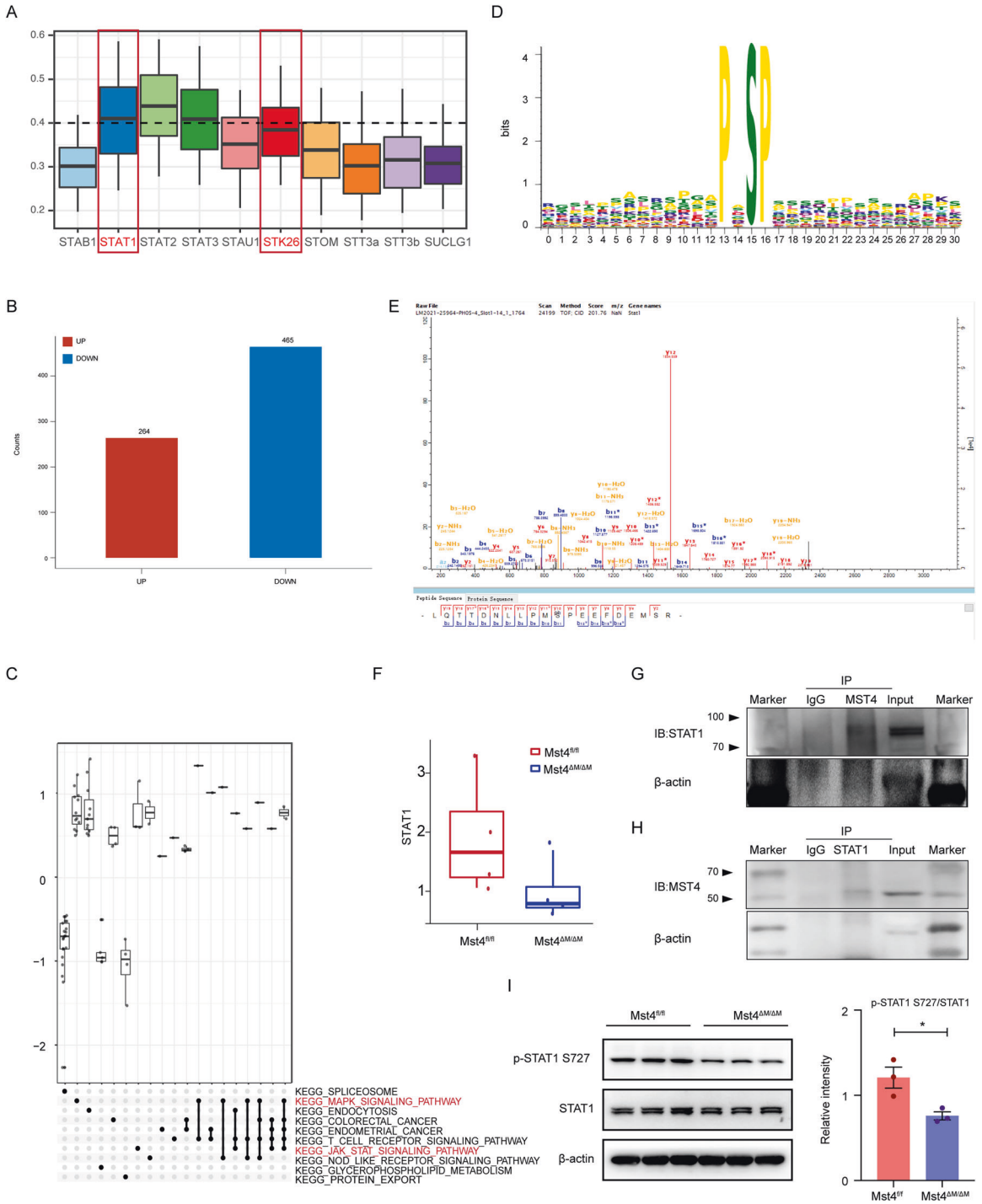

Fig. 6 MST4 promotes the development of M1 macrophages by phosphorylating STAT1. **A** Summary of the functional similarities of the MST4 interactome in M1 macrophages. The lower and upper box boundaries represent the 25th and 75th percentiles, and the line in the box represents the median. The dashed line represents the cutoff value. Proteins with a higher average functional similarity (cutoff > 0.4) were considered central proteins within the MST4 interactome in M1 macrophages. **B** A total of 729 differentially phosphorylated sites were observed in M1 macrophages of *Mst4*$^{fl/fl}$ ITP mice compared with M1 macrophages of *Mst4*$^{\Delta M/\Delta M}$ ITP mice, as revealed by phosphoproteomics data. **C** Kinase-substrate enrichment analysis of the phosphoproteomic data using the clusterProfiler package and kinase-substrate "gene sets" assembled from PhosphoSitePlus. **D** Most common trend of amino acid sequences before and after phosphorylation sites revealed by the protein motif analysis. **E** Phosphorylation profile of STAT1 at Ser727. **F** The phosphorylation of Ser727 at STAT1 was relatively reduced in M1 macrophages from *Mst4*$^{\Delta M/\Delta M}$ ITP mice, as revealed by the phosphoproteomic analysis. Coimmunoprecipitation of STAT1 with MST4 (**G**) and MST4 with STAT1 (**H**) in lysates of M1 macrophages derived from bone marrow cells and incubated with IgG-coated latex beads for 2 h. Left margin, molecular size in kilodaltons. **I** The phosphorylation of Ser727 at STAT1 was reduced in M1 macrophages from *Mst4*$^{\Delta M/\Delta M}$ ITP mice, as revealed by the immunoblot analysis (left), and the quantification of relative intensity (phosphorylation of Ser727 in STAT1 relative to STAT1) is shown (right). β-actin served as the loading control. The data are presented as the means ± SEMs in all the panels. *$p < 0.05$

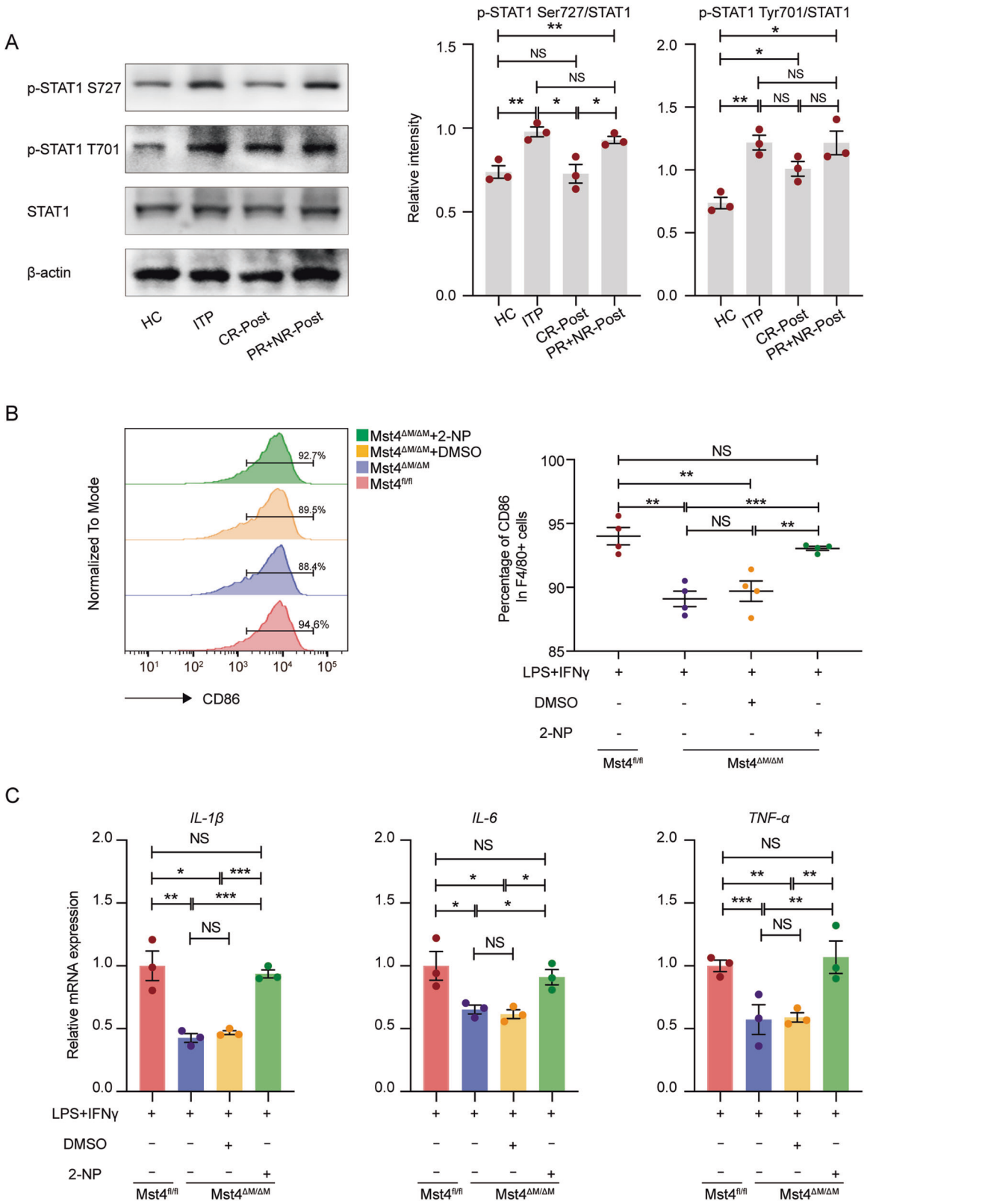

Fig. 7 The activation of STAT1 rescues the compromised development of MST4-deficient M1 macrophages. **A** Immunoblot analysis of STAT1 and p-STAT1 in M1 macrophages induced from the sorted $CD14^{+}$ monocytes of healthy volunteers and ITP patients (left) and quantification of relative intensity (phosphorylated proteins relative to STAT1) (right). β-actin served as the loading control. **B** LPS + IFN-γ-stimulated BMDMs from *Mst4*$^{\Delta M/\Delta M}$ and *Mst4*$^{fl/fl}$ ITP mice were cultured with a specific activator of STAT1 (2-NP, 50 μM). A representative FACS histogram of M1 macrophages and quantification of the percentage of CD86 in macrophages is shown (right). **C** The compromised expression of *Il-1β*, *Il-6*, and *Tnf-α* in M1 macrophages of *Mst4*$^{\Delta M/\Delta M}$ ITP mice was restored to a normal level in the presence of 2-NP. The data are presented as the means ± SEMs in all the panels. *$p < 0.05$, **$p < 0.01$, ***$p < 0.001$

of STAT1 caused by MST4 depletion explained the predominance of FcγRIIb in macrophages. In contrast to activating FcγRs, the expression of inhibitory FcγRIIb is increased by IL-4 and decreased by IFN-γ [58]. The imbalance between inhibitory and activating FcγR expression observed in MST4-knockdown macrophages was also attributed, at least partially, to the lower abundance of IFN-γ caused by compromised M1 activation and thus an ameliorated inflammatory state. In the present study, the protein level of FcγRs in M1 macrophages differed between in vitro and in vivo experiments. Apparently, the destruction of antibody-opsonized platelets by macrophages is influenced by many dynamic factors. In vivo, macrophages reside within a complex environment containing a medium of cell populations and multiple cell-secreted factors, which may not be reflected by in vitro cell culture. It is, however, clear that ablation of *MST4* in macrophages affects the balance of activating and inhibitory FcγRs and subsequently regulates the phagocytic capacity.

We previously reported an inhibitory role for MST4 in LPS-triggered inflammatory responses through the phosphorylation of TRAF6 [30]. The discrepancy between the current observations and our previous study could be attributed to the distinct pathogenic mechanisms underlying ITP and sepsis. The binding of IgG-platelet complexes to FcγRs on macrophages triggers robust inflammatory responses leading to the initiation of ITP [5], whereas the TLR-MyD88 signaling pathway triggered by LPS or bacteria participates in the pathogenesis of sepsis [30]. Additionally, the application of different methodologies or stimulation paradigms may contribute to the discrepancies. IFNγ + LPS and/or antibody-opsonized platelets were used in cellular experiments in the current study to induce the development and trigger functional changes of M1 macrophages, whereas LPS was used alone to initiate sepsis in the previous study. Further investigations are needed to fully elucidate the roles of MST4 in both ITP and inflammatory responses.

In summary, the present study revealed the role and underlying mechanisms of MST4 in the M1 polarization of macrophages and their FcγR-mediated phagocytosis in ITP. The enhanced expression of *MST4* in the expanded M1 macrophages implied a critical role of MST4 in the pathogenesis of ITP. The depletion of MST4 in macrophages attenuated the phosphorylation of STAT1 and compromised the development of M1 macrophages and their phagocytic capacity in ITP. Collectively, our study provides novel insights into the pathogenesis of ITP and highlights MST4 as a potential therapeutic target in ITP.

DATA AVAILABILITY

All data generated or analyzed in this study are included in this published article [and its supplementary information files.

REFERENCES

1. Cooper N, Ghanima W. Immune thrombocytopenia. N Engl J Med. 2019;381:945–55.
2. Hou Y, Xie J, Wang S, Li D, Wang L, Wang H, et al. Glucocorticoid receptor modulates myeloid-derived suppressor cell function via mitochondrial metabolism in immune thrombocytopenia. Cell Mol Immunol. 2022;19:764–76.
3. Zhuang X, Xu P, Ou Y, Shao X, Li Y, Ma Y, et al. Decreased cyclooxygenase-2 associated with impaired megakaryopoiesis and thrombopoiesis in primary immune thrombocytopenia. J Transl Med. 2023;21:540.
4. Shao X, Xu P, Ji L, Wu B, Zhan Y, Zhuang X, et al. Low-dose decitabine promotes M2 macrophage polarization in patients with primary immune thrombocytopenia via enhancing KLF4 binding to PPARγ promoter. Clin Transl Med. 2023;13:e1344.
5. Audia S, Mahevas M, Samson M, Godeau B, Bonnotte B. Pathogenesis of immune thrombocytopenia. Autoimmun Rev. 2017;16:620–32.
6. Bussel J, Cooper N, Boccia R, Zaja F, Newland A. Immune thrombocytopenia. Expert Rev Hematol. 2021;14:1013–25.
7. Semple JW, Rebetz J, Maouia A, Kapur R. An update on the pathophysiology of immune thrombocytopenia. Curr Opin Hematol. 2020;27:423–9.
8. Neunert C, Terrell DR, Arnold DM, Buchanan G, Cines DB, Cooper N, et al. American Society of Hematology 2019 guidelines for immune thrombocytopenia. Blood Adv. 2019;3:3829–66.
9. Ou Y, Zhan Y, Zhuang X, Shao X, Xu P, Li F, et al. A bibliometric analysis of primary immune thrombocytopenia from 2011 to 2021. Neutrophils contribute to elevated BAFF levels to modulate adaptive immunity in patients with primary immune thrombocytopenia by CD62P and PSGL1 interaction. Br J Haematol. 2023;201:954–70.
10. Zhan Y, Cao J, Ji L, Zhang M, Shen Q, Xu P, et al. Impaired mitochondria of Tregs decreases OXPHOS-derived ATP in primary immune thrombocytopenia with positive plasma pathogens detected by metagenomic sequencing. Exp Hematol Oncol. 2022;11:48.
11. Nahrendorf M, Swirski FK. Monocyte and macrophage heterogeneity in the heart. Circ Res. 2013;112:1624–33.
12. Hashimoto D, Miller J, Merad M. Dendritic cell and macrophage heterogeneity in vivo. Immunity. 2011;35:323–35.
13. Gordon S, Pluddemann A, Martinez Estrada F. Macrophage heterogeneity in tissues: phenotypic diversity and functions. Immunol Rev. 2014;262:36–55.
14. Cuccarese MF, Dubach JM, Pfirschke C, Engblom C, Garris C, Miller MA, et al. Heterogeneity of macrophage infiltration and therapeutic response in lung carcinoma revealed by 3D organ imaging. Nat Commun. 2017;8:14293.
15. Udalova IA, Mantovani A, Feldmann M. Macrophage heterogeneity in the context of rheumatoid arthritis. Nat Rev Rheumatol. 2016;12:472–85.
16. Murray PJ, Wynn TA. Protective and pathogenic functions of macrophage subsets. Nat Rev Immunol. 2011;11:723–37.
17. Krausgruber T, Blazek K, Smallie T, Alzabin S, Lockstone H, Sahgal N, et al. IRF5 promotes inflammatory macrophage polarization and TH1-TH17 responses. Nat Immunol. 2011;12:231–8.
18. Feng Q, Xu M, Yu YY, Hou Y, Mi X, Sun YX, et al. High-dose dexamethasone or all-trans-retinoic acid restores the balance of macrophages towards M2 in immune thrombocytopenia. J Thromb Haemost. 2017;15:1845–58.
19. Di Paola A, Palumbo G, Merli P, Argenziano M, Tortora C, Strocchio L, et al. Effects of eltrombopag on in vitro macrophage polarization in pediatric immune thrombocytopenia. Int J Mol Sci. 2020;22:97.
20. Psaila B, Bussel JB. Fc receptors in immune thrombocytopenias: a target for immunomodulation? J Clin Investig. 2008;118:2677–81.
21. Nimmerjahn F, Ravetch JV. Fcgamma receptors as regulators of immune responses. Nat Rev Immunol. 2008;8:34–47.
22. Wijngaarden S, van de Winkel JG, Jacobs KM, Bijlsma JW, Lafeber FP, van Roon JA. A shift in the balance of inhibitory and activating Fcgamma receptors on monocytes toward the inhibitory Fcgamma receptor IIb is associated with prevention of monocyte activation in rheumatoid arthritis. Arthritis Rheum. 2004;50:3878–87.
23. Yu X, Lazarus AH. Targeting FcgammaRs to treat antibody-dependent autoimmunity. Autoimmun Rev. 2016;15:510–2.
24. Liu XG, Ma SH, Sun JZ, Ren J, Shi Y, Sun L, et al. High-dose dexamethasone shifts the balance of stimulatory and inhibitory Fcgamma receptors on monocytes in patients with primary immune thrombocytopenia. Blood. 2011;117:2061–9.
25. Liu XG, Liu S, Feng Q, Liu XN, Li GS, Sheng Z, et al. Thrombopoietin receptor agonists shift the balance of Fcgamma receptors toward inhibitory receptor IIb on monocytes in ITP. Blood. 2016;128:852–61.
26. Huang T, Kim CK, Alvarez AA, Pangeni RP, Wan X, Song X, et al. MST4 phosphorylation of ATG4B regulates autophagic activity, tumorigenicity, and radioresistance in glioblastoma. Cancer Cell. 2017;32:840–55.e8.
27. An L, Nie P, Chen M, Tang Y, Zhang H, Guan J, et al. MST4 kinase suppresses gastric tumorigenesis by limiting YAP activation via a non-canonical pathway. J Exp Med. 2020;217:e20191817.
28. Shi Z, Jiao S, Zhang Z, Ma M, Zhang Z, Chen C, et al. Structure of the MST4 in complex with MO25 provides insights into its activation mechanism. Structure. 2013;21:449–61.
29. Ling P, Lu TJ, Yuan CJ, Lai MD. Biosignaling of mammalian Ste20-related kinases. Cell Signal. 2008;20:1237–47.
30. Jiao S, Zhang Z, Li C, Huang M, Shi Z, Wang Y, et al. The kinase MST4 limits inflammatory responses through direct phosphorylation of the adaptor TRAF6. Nat Immunol. 2015;16:246–57.
31. Liu X, You J, Peng X, Wang Q, Li C, Jiang N, et al. Mammalian Ste20-like kinase 4 inhibits the inflammatory response in Aspergillus fumigatus keratitis. Int Immunopharmacol. 2020;88:107021.
32. Luan D, Zhang Y, Yuan L, Chu Z, Ma L, Xu Y, et al. MST4 modulates the neuroinflammatory response by regulating IkappaBalpha signaling pathway and affects the early outcome of experimental ischemic stroke in mice. Brain Res Bull. 2020;154:43–50.
33. Provan D, Stasi R, Newland AC, Blanchette VS, Bolton-Maggs P, Bussel JB, et al. International consensus report on the investigation and management of primary immune thrombocytopenia. Blood. 2010;115:168–86.

34. Shao X, Wu B, Cheng L, Li F, Zhan Y, Liu C, et al. Distinct alterations of CD68(+) CD163(+) M2-like macrophages and myeloid-derived suppressor cells in newly diagnosed primary immune thrombocytopenia with or without CR after high-dose dexamethasone treatment. J Transl Med. 2018;16:48.
35. Wang J, Xie L, Wang S, Lin J, Liang J, Xu J. Azithromycin promotes alternatively activated macrophage phenotype in systematic lupus erythematosus via PI3K/Akt signaling pathway. Cell Death Dis. 2018;9:1080.
36. Neschadim A, Branch DR. Mouse Models for Immune-Mediated Platelet Destruction or Immune Thrombocytopenia (ITP). Curr Protoc Immunol. 2016;113:15.30.1–15.30.13.
37. Han Y, Yu G, Sarioglu H, Caballero-Martinez A, Schlott F, Ueffing M, et al. Proteomic investigation of the interactome of FMNL1 in hematopoietic cells unveils a role in calcium-dependent membrane plasticity. J Proteom. 2013;78:72–82.
38. Hornbeck PV, Zhang B, Murray B, Kornhauser JM, Latham V, Skrzypek E. PhosphoSitePlus, 2014: mutations, PTMs and recalibrations. Nucleic Acids Res. 2015;43:D512–20.
39. Lawrence T, Natoli G. Transcriptional regulation of macrophage polarization: enabling diversity with identity. Nat Rev Immunol. 2011;11:750–61.
40. Grace RF, Lambert MP. An update on pediatric immune thrombocytopenia (ITP): differentiating primary ITP, IPD, and PID. Blood. 2021.
41. Palandri F, Rossi E, Bartoletti D, Ferretti A, Ruggeri M, Lucchini E, et al. Real-world use of thrombopoietin receptor agonists in older patients with primary immune thrombocytopenia. Blood. 2021;138:571–83.
42. Bolton-Maggs PHB, George JN. Immune thrombocytopenia treatment. N Engl J Med. 2021;385:948–50.
43. Lambert MP, Gernsheimer TB. Clinical updates in adult immune thrombocytopenia. Blood. 2017;129:2829–35.
44. Wang H, Yu T, An N, Sun Y, Xu P, Han P, et al. Enhancing regulatory T-cell function via inhibition of high mobility group box 1 protein signaling in immune thrombocytopenia. Haematologica. 2023;108:843–58.
45. Ni X, Wang L, Wang H, Yu T, Xie J, Li G, et al. Low-dose decitabine modulates myeloid-derived suppressor cell fitness via LKB1 in immune thrombocytopenia. Blood. 2022;140:2818–34.
46. Ehrchen JM, Roth J, Barczyk-Kahlert K. More than suppression: glucocorticoid action on monocytes and macrophages. Front Immunol. 2019;10:2028.
47. Cain DW, Cidlowski JA. Immune regulation by glucocorticoids. Nat Rev Immunol. 2017;17:233–47.
48. Caputo M, Cansby E, Kumari S, Kurhe Y, Nair S, Stahlman M, et al. STE20-type protein kinase MST4 controls NAFLD progression by regulating lipid droplet dynamics and metabolic stress in hepatocytes. Hepatol Commun. 2021;5:1183–200.
49. Ramsauer K, Sadzak I, Porras A, Pilz A, Nebreda AR, Decker T, et al. p38 MAPK enhances STAT1-dependent transcription independently of Ser-727 phosphorylation. Proc Natl Acad Sci USA. 2002;99:12859–64.
50. Dhodapkar KM, Banerjee D, Connolly J, Kukreja A, Matayeva E, Veri MC, et al. Selective blockade of the inhibitory Fcgamma receptor (FcgammaRIIB) in human dendritic cells and monocytes induces a type I interferon response program. J Exp Med. 2007;204:1359–69.
51. Allan SM, Tyrrell PJ, Rothwell NJ. Interleukin-1 and neuronal injury. Nat Rev Immunol. 2005;5:629–40.
52. Xu D, Mu R, Wei X. The roles of IL-1 family cytokines in the pathogenesis of systemic sclerosis. Front Immunol. 2019;10:2025.
53. Heinrich PC, Behrmann I, Haan S, Hermanns HM, Müller-Newen G, Schaper F. Principles of interleukin (IL)-6-type cytokine signalling and its regulation. Biochem J. 2003;374:1–20.
54. Sica A, Mantovani A. Macrophage plasticity and polarization: in vivo veritas. J Clin Investig. 2012;122:787–95.
55. Chen S, Saeed A, Liu Q, Jiang Q, Xu H, Xiao GG, et al. Macrophages in immunoregulation and therapeutics. Signal Transduct Target Ther. 2023;8:207.
56. Samuelsson A, Towers TL, Ravetch JV. Anti-inflammatory activity of IVIG mediated through the inhibitory Fc receptor. Science. 2001;291:484–6.
57. Panchanathan R, Shen H, Duan X, Rathinam VA, Erickson LD, Fitzgerald KA, et al. Aim2 deficiency in mice suppresses the expression of the inhibitory Fcgamma receptor (FcgammaRIIB) through the induction of the IFN-inducible p202, a lupus susceptibility protein. J Immunol. 2011;186:6762–70.
58. Pricop, Redecha L, Teillaud P, Frey JL, Fridman J, Sautes WH, et al. Differential modulation of stimulatory and inhibitory Fc gamma receptors on human monocytes by Th1 and Th2 cytokines. J Immunol. 2001;166:531–7.

ACKNOWLEDGEMENTS

This study was conducted at the Institute of Clinical Science of Zhongshan Hospital, Fudan University. The study was supported by the Medical Science Data Center of Shanghai Medical College of Fudan University. We sincerely thank all staff and participants for their important contributions.

AUTHOR CONTRIBUTIONS

YC, ZZ, JC, LJ, YZ, and HC performed the literature review and drafted and revised the manuscript; JC, YC, HC, and ZZ contributed to the critical revision of the manuscript; YZ, LJ, PX, HC, YO, XZ, XS, BW, PC, LC, LS, FH, FL, and YC performed the experiments and analyzed the data. All the authors have read and approved the final manuscript.

FUNDING

This work was supported by grants from the National Natural Science Foundation of China (82370130, 81870098, 82300146), the Program of the Shanghai Academic/Technology Researcher Leader (20XD1401000), the Shanghai Engineering Research Center of Tumor Multi-Target Gene Diagnosis (20DZ2254300), the Key Subject Construction Program of the Shanghai Health Administrative Authority (ZK2019B30), and the Science and Technology Commission of the Shanghai Municipality (21ZR1459000). All authors obtained permission to acknowledge all those mentioned in the acknowledgments.

COMPETING INTERESTS

The authors declare no competing interests.

ETHICS APPROVAL AND CONSENT TO PARTICIPATE

The study was in accordance with the ethical standards formulated in the Helsinki Declaration and was approved by the respective local Medical Ethics Committees of Zhongshan Hospital of Fudan University (#B2020-279R). Written informed consent was obtained from each patient upon enrollment.

ADDITIONAL INFORMATION

Supplementary information The online version contains supplementary material available at https://doi.org/10.1038/s41423-023-01089-8.

Correspondence and requests for materials should be addressed to Hao Chen, Zhaocai Zhou or Yunfeng Cheng.

Supplementary information: The online version contains supplementary material available at https://doi.org/10.1038/s41423-023-01089-8.